

Low-Cost Phase Precoding for Short-Reach Fiber Links with Direct Detection

Ulrike Höfler, Daniel Plabst and Norbert Hanik, *Senior Member, IEEE*

Abstract—Low-cost analog phase precoding is used to compensate chromatic dispersion (CD) in fibers with intensity modulation and direct detection (IM/DD). In contrast to conventional precoding with an in-phase and quadrature (IQ) Mach-Zehnder modulator (MZM), only a single additional phase modulator (PM) is required at the transmitter. Depending on the CD, the PM generates a periodic phase modulation that is modelled by a Fourier series and optimized via a mean squared error (MSE) cost criterion. Numerical results compare achievable information rates (AIRs) for 4- and 6-PAM. With the additional PM, energy gains of up to 3 dB are achieved for moderate fiber lengths.

Index Terms—intensity modulation/direct detection, short-reach fiber-optic, phase precoding, chromatic dispersion

I. INTRODUCTION

Short-reach fiber-optic links with several to tens of kilometers are commonly used to connect data centers and metropolitan areas [1], [2]. To reduce hardware cost, these systems often use a direct detection (DD) receiver, which has a single photo-diode (PD) performing the optical to electrical conversion [3]. Short-reach fiber links with DD are mainly impaired by intersymbol interference (ISI) due to chromatic dispersion (CD), and the nonlinear squaring due to the PD [2].

Dispersion can be compensated electrically or optically. Optical compensation techniques, such as dispersion compensating fibers (DCFs) add significant link loss [4], [5] and additional hardware cost. In the electric domain, one may compensate dispersion via receiver equalization or transmitter precoding. We briefly discuss these methods in the following subsections I-A and I-B.

A. Equalization

Electronic linear equalizers [6] cannot cancel the nonlinear squaring operation of the PD and lose rate at high-SNR. Non-linear equalizers such as decision feedback equalizers (DFEs), Volterra filters, forward-backward algorithm (FBA) equalizers or neural network (NN) equalizers [7] show good performance in general. However, DFEs lead to error propagation and add complexity via an additional feedback filter [8]. Volterra filters and FBA-based approaches are generally complex. NN-based equalization [7] shows good rate and complexity improvements, but simpler compensation techniques may be preferred for low-cost and low-latency short-reach links with DD.

B. Precoding

One may precode the transmit signal to compensate the complex-valued CD. The papers [9]–[12] use coherent precoding with two Mach-Zehnder modulators (MZM) and compensate the CD electrically via linear transmitter zero-forcing. To reduce hardware cost, [13] performs CD compensation with a single dual-drive MZM. The approach is interference-limited, as the dual-drive configuration does not allow independent precoding of the signal amplitude and phase, and thus cannot fully precompensate the CD. The authors of [14] consider hybrid optical and electrical CD compensation for Gaussian transmit pulses. A fiber Bragg grating (FBG) is used to optically precompensate a major part of the CD. Subsequently, an electrically tuneable phase modulator (PM) is configured to remove the remaining dispersion.

Other works use directly modulated lasers (DMLs) or electro-absorption modulated lasers (EMLs) for intensity modulation [15]–[20]. In IM systems, DMLs introduce a time-dependent phase to the bandpass signal, which is proportional to both the output power and the rate of change in output power. In contrast, EMLs introduce phase modulation that depends solely on the rate of change in output power [1, Sec. 2.1]. Notably, this generated time-varying phase can be exploited for partial precompensation of CD. For low data rates around 10 Gbit/s, the authors of [21] use the time-dependent phase introduced by the DML for symbol-wise phase precoding in combination with an electro-absorption modulator (EAM) for IM. However, the performance of DMLs is significantly affected by intrinsic characteristics such as modulation efficiency and residual intensity modulation, limiting their suitability for this approach at higher data rates [22]–[26]. The paper [16] uses an EML with an optimized operating point to mitigate the effects of CD. Additionally, the authors of [27] jointly optimize the DML and EAM for modulation and CD compensation. At high data rates, however, additional receiver equalization is required to compensate the interaction between the nonlinear modulators, the larger CD and the PD [1]. EMLs, for instance, exhibit stronger nonlinear behavior at higher IM levels because the resulting time-dependent phase varies with different modulation voltage levels, leading to further nonlinear distortions when interacting with the CD. Similarly, for DMLs, the introduced phase modulation creates a power-dependent carrier frequency shift, which is converted into additional nonlinear distortions by CD [1, Sec. 2.2].

U. Höfler, D. Plabst and N. Hanik are with the Institute for Communications Engineering, Technical University of Munich, 80333 Munich, Germany (e-mail: {ulrike.hoeffler, daniel.plabst, norbert.hanik}@tum.de).

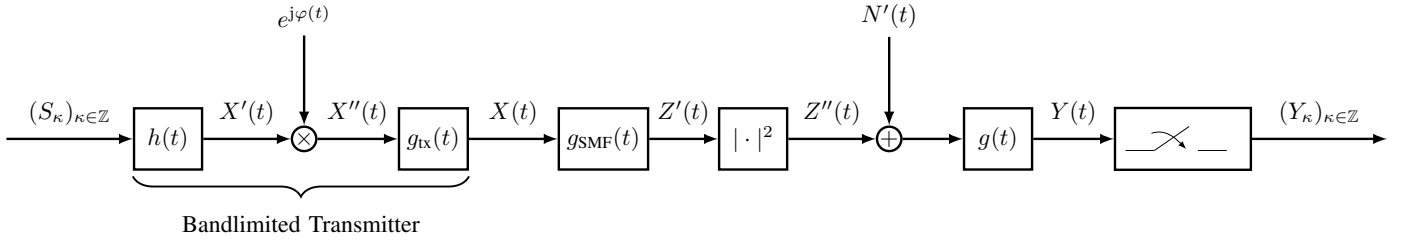


Fig. 1. Baseband model of the considered short reach optical communication system.

C. Contributions and Organization

This paper considers low-cost analog phase precoding for CD compensation. The transmitter uses a single MZM for amplitude modulation, followed by a PM that performs symbol-wise periodic phase precoding. The phase precoding depends on the total CD, transmit filter, the statistics of the transmit constellation and the receive filter. The periodic control signal to the PM may be generated via low-cost analog circuits, e.g., oscillators, frequency doublers and operational amplifiers.

In contrast to [14], we model the periodic phase by a Fourier series and obtain a closed-form expression of the mean-squared error (MSE) between transmitted and received symbols. The coefficients of the PM are optimized for frequency domain raised cosine (FD-RC) and time domain raised cosine pulses (TD-RC) as well as 4- and 6-PAM.

The paper [28] shows that a MZM and a PM can be integrated in a single compact and low-loss modulator package. Thus, the presented precompensation scheme may be a good candidate for practical systems.

D. Notation

Matrices and vectors are written using bold letters, e.g., \mathbf{x} . The transpose, complex conjugate, and complex conjugate transpose (Hermitian) of \mathbf{x} are \mathbf{x}^T , \mathbf{x}^* and \mathbf{x}^H , respectively. The Hadamard product between vectors \mathbf{x} and \mathbf{y} is written as $\mathbf{x} \circ \mathbf{y}$. We use $|\mathbf{x}|$ to denote the element-wise absolute value of \mathbf{x} and $\mathbf{x}^{\circ 2}$ denotes element-wise squaring.

By $\mathbf{A} = \text{diag}(\mathbf{a})$ we denote a diagonal matrix that has \mathbf{a} on its diagonal, while $\mathbf{a} = \text{diag}(\mathbf{A})$ arranges the diagonal entries of \mathbf{A} in the column vector \mathbf{a} . The $N \times N$ -dimensional identity matrix is denoted as \mathbf{I}_N and the N -dimensional all-ones column vector is $\mathbf{1}_N$. By \mathbf{e}_i we denote the unit column vector that contains zeros everywhere, except at position $i + 1$, where it contains a one.

We define the sinc function as $\text{sinc}(t) = \sin(\pi t)/(\pi t)$. The Fourier transform of the signal $x(t)$ is defined as $\mathcal{F}\{x(t)\}(f) = \int_{-\infty}^{\infty} x(t)e^{-j2\pi ft} dt$ and convolution between two signals $x(t)$ and $y(t)$ is written as $(x * y)(t)$.

II. SYSTEM MODEL

A. Continuous-Time Model

Figure 1 shows the considered short-reach fiber-optic system. The transmit symbols $(S_\kappa)_{\kappa \in \mathbb{Z}}$ are uniformly, independently and identically distributed M -PAM symbols with alpha-

bet $\mathcal{A}_M = \{a_0, \dots, a_{M-1}\}$. The digital-to-analog converter (DAC) performs pulse shaping with $h(t)$ and generates

$$X'(t) = \sum_{\kappa \in \mathbb{Z}} S_\kappa h(t - \kappa T_s) \quad (1)$$

with symbol rate $B = 1/T_s$. We focus on pulses $h(t)$ that are either FD-RC or TD-RC pulses with a roll-off factor of α_{ps} . For instance, choosing FD-RC with $\alpha_{\text{ps}} = 0$ gives the sinc pulse

$$h(t) = \text{sinc}(t/T_s) \quad (2)$$

with single-sided bandwidth $B/2$ [29, Eq. (6.17)], whereas choosing TD-RC¹ with $\alpha_{\text{ps}} = 0$ corresponds to a rectangular pulse

$$h(t) = \begin{cases} 1, & |t| \leq T_s/2 \\ 0, & \text{otherwise.} \end{cases} \quad (3)$$

The pulse-shaped signal is precoded with a PM

$$X''(t) = X'(t) e^{j\varphi(t)}. \quad (4)$$

The choice of $\varphi(t)$ is discussed in the next subsection. We assume the transmitter to be band-limited, as this is useful for wavelength division multiplexing applications. The band limitation is modeled by a low-pass filter $G_{\text{tx}}(f)$ and for simplicity we choose the brickwall filter

$$G_{\text{tx}}(f) = \begin{cases} 1, & |f| \leq B_{\text{tx}}/2 \\ 0, & \text{otherwise.} \end{cases} \quad (5)$$

The low-pass filtered transmit signal $X(t)$ passes through the linear fiber channel (6) with the baseband transfer function:

$$H_{\text{SMF}}(f) = e^{-j\frac{\beta_2}{2}(2\pi f)^2 L} e^{-\frac{\alpha_{\text{SMF}}}{2} L}, \quad (6)$$

where β_2 is the chromatic dispersion coefficient, α_{SMF} the attenuation coefficient and L the fiber length.

At the receiver, a PD performs an optical-to-electrical conversion and generates $Z''(t) = |Z'(t)|^2$. We consider the PD at the thermal noise limit, where stationary real Gaussian noise $N'(t)$ with a two-sided power spectral density (PSD) of $\Phi_{N'}(f) = N_0/2$ is added; see Fig. 1.

The receive filter limits the noise power and is modelled as a unit-gain brickwall filter $g(t)$ with two-sided bandwidth B_{rx} .

¹A TD-RC pulse is obtained by swapping (t, T_s) and (f, B) in [29, Eq. (6.17)]

The noise $N(t) = (g * N')(t)$ is colored zero-mean Gaussian with average power $\sigma_N^2 = B_{\text{rx}} \cdot N_0/2$ and PSD

$$\Phi_N(f) = |G(f)|^2 \Phi_{N'}(f) = \begin{cases} \frac{N_0}{2}, & |f| \leq B_{\text{rx}}/2 \\ 0, & \text{otherwise.} \end{cases} \quad (7)$$

B. Phase Modulator

We choose an even, T_s -periodic phase $\varphi(t)$, expressed via the Fourier series²:

$$\varphi(t) = \sum_{w=1}^W \eta_w \cos(2\pi w t B) \quad (8)$$

with coefficients $\eta_w \in \mathbb{R}$ for $w \in \{1, \dots, W\}$. The W coefficients adjust the phase modulation; see Fig. 2. Phase pre-coding, being inherently nonlinear, causes spectral expansion. The Fourier transform of (4) is

$$X''(f) = \left(X' * \mathcal{F} \left\{ \exp(j\varphi(t)) \right\} \right)(f). \quad (9)$$

We use (8) in (9) to compute the frequency response of the phase modulation

$$\begin{aligned} \mathcal{F} \{ e^{j\varphi(t)} \}(f) &= \mathcal{F} \left\{ \prod_{w=1}^W e^{j\eta_w \cos(2\pi w t B)} \right\}(f) \\ &= \underbrace{(\Omega_1 * \dots * \Omega_w * \dots * \Omega_W)}_{W \times}(f), \end{aligned} \quad (10)$$

where the last step follows from the Jacobi-Anger expansion for complex exponentials

$$e^{j\eta_w \cos(2\pi w t B)} = \sum_{u \in \mathbb{Z}} j^u J_u(\eta_w) e^{j2\pi u w t B} \quad (11)$$

and the Fourier transform of (11):

$$\Omega_w(f) = \sum_{u \in \mathbb{Z}} j^u J_u(\eta_w) \delta(f - w u B), \quad (12)$$

where the Bessel function of the first kind of u -th order is denoted by $J_u(\eta_w)$.

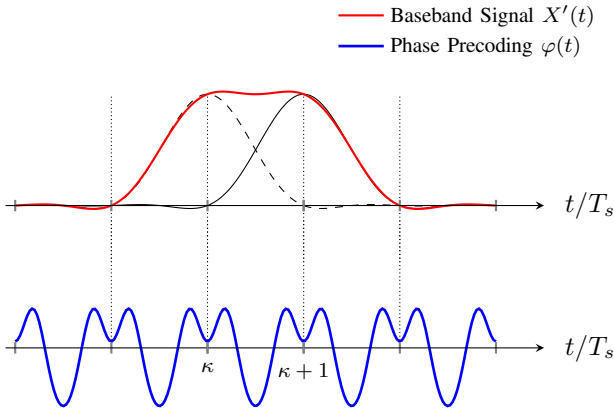


Fig. 2. Example of a baseband signal $X'(t)$ with FD-RC $\alpha_{\text{ps}} = 1$ and symbols $(+1, +1)$ at times $(\kappa, \kappa + 1)$. The analog phase pre-coding $\varphi(t)$ is T_s -periodic, exemplarily with $\eta_i \neq 0$, $i \in \{1, 2\}$.

²We dropped the constant η_0 , as the PD output $Z''(t)$ is invariant to constant phase rotations. We also neglect the $\sin(\cdot)$ terms in the Fourier series, as optimizing the associated weights corresponding to section III results in zero weighting.

As an example, consider the phase pre-coding (8) with one non-zero Fourier coefficient (η_1). The spectrum

$$X''(f) = \sum_{u \in \mathbb{Z}} j^u J_u(\eta_1) X'(f - uB) \quad (13)$$

has unbounded bandwidth, as weighted spectral replica of the baseband signal $X'(f)$ appear centered at uB , see (12).

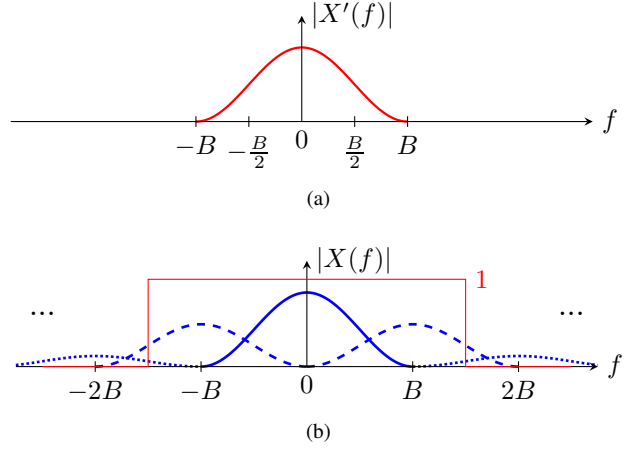


Fig. 3. Spectrum of a FD-RC $\alpha_{\text{ps}} = 1$: (a) before phase pre-coding and (b) after phase pre-coding. The frequency response of a transmit filter with bandwidth $B_{\text{tx}} = 3B$ is shown in red.

Applying the filter(5) to (9) results in

$$X(f) = G_{\text{tx}}(f) \sum_{u^W} \left(\prod_{i=1}^W j^{u_i} J_{u_i}(\eta_i) \right) X' \left(f - B \sum_{i=1}^W i u_i \right), \quad (14)$$

where $u^W := (u_1, \dots, u_W)$ and $u_i \in \mathbb{Z}$ for $i = \{1, \dots, W\}$. We set the bandwidth of (5) to $B_{\text{tx}} := B(2F - 1)$ and $F \in \mathbb{N}^+$. For instance, for a transmit signal spectrum $X'(f)$ that is bandlimited to $|f| \leq B$, setting $F = 2$ will produce a PM output $X(f)$ depending on the four weighted spectral copies of $X'(f)$ centered at $f \in \{\pm B, \pm 2B\}$; see Fig. 3.

C. Discrete-Time Model

To obtain a low-complexity receiver, we sample $Y(t)$ at symbol rate³, i.e., we set $t = \kappa T_s$, $\kappa \in \mathbb{Z}$.

$$Y_\kappa = Z_\kappa + N_\kappa, \quad (15)$$

where

$$Z_\kappa = [g(t) * |Z'(t)|^2]_{t=\kappa T_s} \quad (16)$$

$$N_\kappa = [g(t) * N'(t)]_{t=\kappa T_s}. \quad (17)$$

In general, the noise N_κ is a real-valued discrete-time colored Gaussian process with ACF $\varphi_{\text{NN}}[\kappa] = \sigma_N^2 \cdot g(\kappa T_s)$.

³If the filtered signal $Y(t)$ occupies a larger bandwidth than B , sampling at symbol rate may not result in sufficient statistics and may thus cause an achievable rate loss; see [30, Fig. 7]. One can find a trade-off between rate loss and receiver complexity.

D. Approximation via Simulation

In order to obtain a discrete-time model for the channel inputs $(S_\kappa)_{\kappa \in \mathbb{Z}}$ and outputs $(Z_\kappa)_{\kappa \in \mathbb{Z}}$, caution is required due to the bandwidth expansion of the nonlinear PM and PD.

The bandwidth of the PM output signal $X''(t)$ is in general unbounded, see (13). The additional filter $g_{\text{tx}}(t)$ ensures that $X(t)$ is bandlimited to $\pm B_{\text{tx}}/2$; see Fig. 3. Since the fiber is assumed to be linear, no spectral broadening takes place. Finally, the PD squaring operation doubles the bandwidth of $Z''(t)$ to $\pm B_{\text{tx}}$. We use oversampling to address these bandwidth expansions; see [7, Sec. II. D].

Assume oversampling with factor N_{os} and corresponding sampling period $T_{\text{sim}} = T_s/N_{\text{os}}$. The noise-free channel outputs are

$$Z_\kappa = \sum_{\ell_1 \in \mathbb{Z}} g_{\ell_1} \left| \sum_{\ell_2 \in \mathbb{Z}} g_{\text{SMF}, \ell_2} X_{\kappa N_{\text{os}} - \ell_1 - \ell_2} \right|^2 \quad (18)$$

where $g_\ell := g(\ell T_{\text{sim}})$, $g_{\text{SMF}, \ell} := g_{\text{SMF}}(\ell T_{\text{sim}})$, and $X_\ell := X(\ell T_{\text{sim}})$. The expansion (14) gives insight into the spectrum of the PM output $X(t)$: As an example, consider $W = 1$, a bandlimited DAC signal $X'(t)$ on $|f| \leq B/2$ and finite B_{tx} . In this case we may simplify (14) to

$$X(f) = \sum_{u \in \mathbb{Z}: |u| \leq B_{\text{tx}}/(2B)} j^u J_u(\eta_1) X'(f - Bu). \quad (19)$$

One may generate discrete-time representations X_ℓ from the bandlimited (19). Unfortunately, for $W \geq 2$, the summation in (14) is over infinitely many terms, which is unpractical. Furthermore, for TD-RC pulses, the DAC signal $X'(t)$ is unbounded in frequency. Thus, for the general case, we approximate the bandlimited PM signal as

$$X_\ell \approx \sum_{\ell_1 \in \mathbb{Z}} g_{\text{tx}, \ell_1} e^{j\varphi_{\ell_1 - \ell}} \sum_{\ell_2 \in \mathbb{Z}} h_{\ell_2} S'_{\ell - \ell_1 - \ell_2} \quad (20)$$

with $g_{\text{tx}, \ell} := g_{\text{tx}}(\ell T_{\text{sim}})$, $\varphi_\ell := \varphi(\ell T_{\text{sim}})$, $h_\ell := h(\ell T_{\text{sim}})$, and the N_{os} -fold upsampled symbol sequence $(S'_\ell)_{\ell \in \mathbb{Z}} := ((0, \dots, 0), S_\kappa)_{\kappa \in \mathbb{Z}}$. Eq. (20) is an approximation, as the PM signal $X''(t)$ has unbounded bandwidth in general⁴.

Note that (18) requires $N_{\text{os}} \geq 2B_{\text{tx}}/B$ due to the squaring operation of the PD, while (20) may require a much larger oversampling factor. In the numerical results section, we choose $N_{\text{os}} \gg 2B_{\text{tx}}/B$ based on a distortion criterion, which ensures that both (18) and (20) are accurate.

III. OPTIMIZATION VIA MSE

Next, we formulate an MSE objective function for optimizing $\boldsymbol{\eta} := (\eta_i)_{i=1}^W$. We add a real-valued scaling parameter ξ to the MSE cost function ϵ to take fiber attenuation into account. The scaling parameter can be interpreted as an automatic gain control. We define the MSE between a single transmitted and received symbol as

$$(\boldsymbol{\eta}^*, \xi^*) = \arg \min_{\boldsymbol{\eta}, \xi} \epsilon, \quad \epsilon := \mathbb{E} [(S_\kappa - \xi \cdot Y_\kappa)^2]. \quad (21)$$

Next, we formulate Y_κ using the matrix-vector representations of (18) and (20). First, combine the transmit filter and fiber

channel into $f(t) := (g_{\text{tx}} * h_{\text{SMF}})(t)$. Assume that the taps $h_\ell, f_\ell := f(\ell T_{\text{sim}})$ and g_ℓ are zero outside some interval and define the vectors

$$\mathbf{f} := [f_{+(M_f-1)/2}, \dots, f_0, \dots, f_{-(M_f-1)/2}]^T \in \mathbb{C}^{M_f} \quad (22)$$

$$\mathbf{g} := [g_{+(M_g-1)/2}, \dots, g_0, \dots, g_{-(M_g-1)/2}]^T \in \mathbb{R}^{M_g} \quad (23)$$

$$\mathbf{h} := [h_{+(M_h-1)/2}, \dots, h_0, \dots, h_{-(M_h-1)/2}]^T \in \mathbb{R}^{M_h} \quad (24)$$

respectively, where M_h, M_f and M_g are odd integers.

Define the Toeplitz matrix $\mathbf{F} \in \mathbb{C}^{M_g \times M_g + M_f - 1}$ that is constructed from right-shifted copies of \mathbf{f}^T . In the same fashion, the matrix $\mathbf{H}' \in \mathbb{R}^{M_g + M_f - 1 \times Q}$, $Q := M_g + (M_f - 1) + (M_h - 1)$ is constructed from right-shifted copies of \mathbf{h}^T .

The channel outputs are

$$Y_\kappa = \mathbf{g}^T |\mathbf{F} (\exp(j\varphi') \circ (\mathbf{H}' \mathbf{S}'_\kappa))|^2 + N_\kappa, \quad (25)$$

with the upsampled sequence

$$\mathbf{S}'_\kappa = [\underbrace{(S_{\kappa+i}, \mathbf{0})}_{\text{Repeat } i = -B_1, \dots, 1}, S_\kappa, \underbrace{(\mathbf{0}, S_{\kappa+i})}_{\text{Repeat } i = 1, \dots, B_1}]^T \quad (26)$$

where $\mathbf{0} := \mathbf{0}_{N_{\text{os}}-1}^T$ and the periodically repeating phases

$$\varphi' = [\underbrace{(\varphi_0, \varphi_1 \dots \varphi_{N_{\text{os}}-1})}_{\text{Repeat } B_2 \text{ times}}, \varphi_0, \underbrace{(\varphi_1, \dots, \varphi_{N_{\text{os}}-1}, \varphi_0)}_{\text{Repeat } B_2 \text{ times}}]^T. \quad (27)$$

and integers B_1, B_2 that satisfy⁵ the filter lengths (22)-(24). Finally, we express the phase samples $\varphi_\ell, \ell \in \{0, \dots, N_{\text{os}}-1\}$ by the inner product $\varphi_\ell = \boldsymbol{\eta}^T \boldsymbol{\gamma}_\ell$, $\boldsymbol{\eta} := [\eta_1, \dots, \eta_W]^T$ and $\boldsymbol{\gamma}_\ell := [\cos(2\pi\ell/N_{\text{os}}), \dots, \cos(2\pi W\ell/N_{\text{os}})]^T$.

In (25), we simplify the product $\mathbf{H}' \mathbf{S}'_\kappa = \mathbf{H} \mathbf{S}_\kappa$, i.e., we removed the columns in \mathbf{H}' that are multiplied by a zero in \mathbf{S}'_κ and defined $\mathbf{S}_\kappa := [S_{\kappa-B_1}, \dots, S_{\kappa+B_1}]^T$, $\mathbf{H} \in \mathbb{R}^{(M_f + M_g - 1) \times K}$ and $K = (2B_1 + 1)$.

We first optimize the scaling parameter ξ by setting the derivative

$$\frac{\partial \epsilon}{\partial \xi} = -2 \mathbb{E} [S_\kappa Y_\kappa] + 2 \xi \mathbb{E} [Y_\kappa^2] \quad (28)$$

equal to zero and solving for ξ , which results in the optimal

$$\xi^* = \mathbb{E} [S_\kappa Y_\kappa] / \mathbb{E} [Y_\kappa^2]. \quad (29)$$

Insert (29) into ϵ to obtain

$$\epsilon = \mathbb{E} [S_\kappa^2] - \mathbb{E} [S_\kappa Y_\kappa]^2 / \mathbb{E} [Y_\kappa^2], \quad (30)$$

where Y_κ is a function of $\boldsymbol{\eta}$, and $\mathbb{E} [S_\kappa^2]$ is a constant with respect to $\boldsymbol{\eta}$ and can be neglected in the optimization.

When transmitting M -PAM, the elements in \mathcal{A}_M are equidistant, while the noise-free channel outputs are not equidistantly spaced due to the PD squaring. Under AWGN, and at high-SNRs, equidistantly spaced channel outputs maximize the information rates. To create approximately equidistant channel outputs, we extend Fig. 1 by incorporating the square-root predistortion from [6] and transmit $\sqrt{S_\kappa} \in \sqrt{\mathcal{A}_M} := \{\sqrt{a_0}, \dots, \sqrt{a_{M-1}}\}$; see Fig. 4. In principle, one can also optimize the constellation spacing for every SNR, which is called geometric shaping.

⁴For the values of η_w considered in the numerical results, we saw through simulations that the weighting factors $J_u(\eta_w)$ decay quickly.

⁵Alternatively, we pad these filters with zeros on both sides.

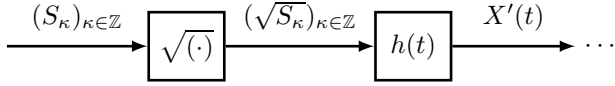


Fig. 4. Transmitter with symbol-wise predistortion.

Define $\Psi := \mathbf{F} \text{diag}(\exp(j\varphi')) \mathbf{H}$. Using the approximation [6, Sec. IV. A, B], we obtain the expected values

$$\begin{aligned} \mathbb{E}[S_\kappa Y_\kappa] &= \mathbf{g}^\top \mathbb{E}[S_\kappa \cdot |\mathbf{F}[\exp(j\varphi') \circ (\mathbf{H} \sqrt{\mathbf{S}_\kappa})]|^2] \\ &= \mathbf{g}^\top \mathbb{E}[S_\kappa \cdot |\Psi \sqrt{\mathbf{S}_\kappa}|^2] \\ &\approx \mathbf{g}^\top \left(\mu_S^2 |\mathbf{w}|^2 + \frac{\sigma_S^2}{4} \mathbf{z} + \sigma_S^2 \text{Re}\{\mathbf{w}^* \circ (\Psi \mathbf{e}_{B_1})\} \right) \end{aligned} \quad (31)$$

and

$$\mathbb{E}[Y_\kappa^2] = \mathbf{g}^\top \underbrace{\mathbb{E}[|\Psi \sqrt{\mathbf{S}_\kappa}|^2 |\Psi \sqrt{\mathbf{S}_\kappa}|^{2,\top}]}_{(a)} \mathbf{g} + \sigma_N^2, \quad (32)$$

where the term (a) is approximated by

$$\begin{aligned} &\mu_S^2 (|\mathbf{w}|^2 |\mathbf{w}|^{2,\top}) \\ &+ \frac{\sigma_S^2}{2} (\text{Re}\{\text{diag}(\mathbf{w}^*) \Psi \Psi^\top \text{diag}(\mathbf{w}^*)\} \\ &\quad + \text{Re}\{\text{diag}(\mathbf{w}^*) \Psi \Psi^H \text{diag}(\mathbf{w})\}) \\ &+ \frac{\sigma_S^2}{4} (\mathbf{z} |\mathbf{w}|^{2,\top} + |\mathbf{w}|^2 \mathbf{z}^\top) \\ &+ \frac{\sigma_S^4}{16 \mu_S^2} (|\Psi \Psi^\top|^2 + |\Psi \Psi^H|^2 + \mathbf{z} \mathbf{z}^\top) \\ &+ \frac{\mu_{4,S} - 3 \sigma_S^4}{16 \mu_S^2} (|\Psi|^2 |\Psi|^{2,\top}), \end{aligned} \quad (33)$$

see [6, Sec. IV. A, B], and $\mathbf{w} := \Psi \mathbf{1}_K$, $\mathbf{z} := |\Psi|^2 \mathbf{1}_K$. The mean, variance and the fourth order central moment of the random variable S are denoted by μ_S , σ_S^2 and $\mu_{4,S} = \mathbb{E}[(S - \mu_S)^4]$, respectively. The gradient $\partial \epsilon / \partial \boldsymbol{\eta}$ of dimension \mathbb{R}^W is provided in the appendix.

IV. SIMULATION RESULTS

The numerical simulations were carried out at a carrier wavelength of $\lambda_c = 1550 \text{ nm}$ with dispersion coefficient $D = 17 \frac{\text{ps}}{\text{nm} \cdot \text{km}}$ and attenuation factor $\alpha_{\text{SMF}} = 0.2 \frac{\text{dB}}{\text{km}}$. The Kerr nonlinearity is neglected. To modulate the signal, {4,6}-PAM modulation is used with alphabets $\mathcal{A}_4 = \{0, 1, 2, 3\}$ and $\mathcal{A}_6 = \{0, 1, 2, 3, 4, 5\}$, respectively. We choose a symbol rate of 33 GBaud, and use the predistortion in Fig. 4. The simulation oversampling factor is $N_{\text{os}} = 50$ for $W \leq 2$ ensuring that the approximation (20) has a negligible error. The transmitter is bandlimited, i.e., we set $F = 2$ which results in $B_{\text{tx}} = 3B$; see below (14). The average optical power launched into the fiber is

$$P_{\text{tx}} = \lim_{T \rightarrow \infty} \frac{1}{T} \mathbb{E} [\|X(t)\|^2]. \quad (34)$$

The receive filter $g(t)$ models two low-pass filters, i.e., $g(t) = (g_{\text{PD}} * g_{\text{N}})(t)$, where $g_{\text{PD}}(t)$ is the electrical bandwidth limitation of the PD with one-sided bandwidth $B_{\text{PD}}/2 = 50 \text{ GHz}$

and the brickwall filter $g_{\text{N}}(t)$ is adapted to the used pulse shape and passes 99% of the energy of $Z''(t)$. We measure the noise power $B_{\text{PD}} \cdot N_0/2$ directly after the PD filter, and normalize $B_{\text{PD}} \cdot N_0/2 = 1$. Thus, $\text{SNR} = P_{\text{tx}}$. Finally, an analog-to-digital converter (ADC) samples at symbol rate B .

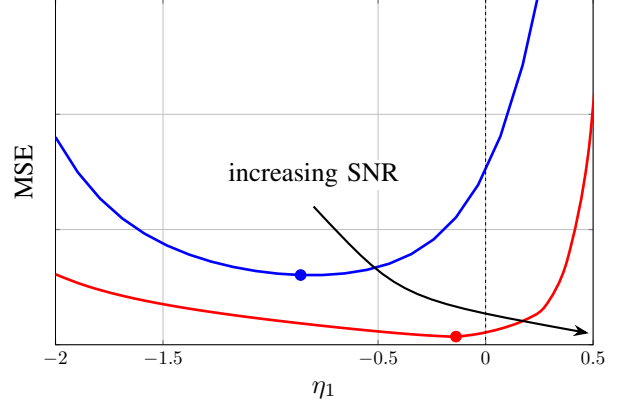


Fig. 6. MSE at 5 km for low- and high-SNR as a function of η_1 ($W = 1$) using FD-RC pulse shaping. The respective minimum is marked with \bullet .

To determine the MSE-optimal coefficients $\boldsymbol{\eta}^*$ for the fiber length L , we use the classic gradient-descent algorithm. We find $\boldsymbol{\eta}^*$ for each SNR. Figure 6 shows the SNR dependency of the MSE, illustrating that the optimized coefficient η_1^* depends on the SNR. At low SNRs, the MSE is slightly flatter around the minimum, owed to the dominant noise. At high-SNR the noise has less impact and chromatic dispersion (CD) takes over as the primary source of distortion. When $\eta_1 > 0$, the effects of CD are enhanced, leading to a significant increase in the MSE.

A. Numerical Results

We compute achievable information rates (AIRs) [31] as the performance metric. These rates are a lower bound on the mutual information rate, and achievable via mismatched decoding with memoryless Gaussian decoding metrics. Although AIRs are not equivalent to the MSE, one can show via [30, Eq. (46)] that minimizing the MSE increases the AIRs.

Figure 5 shows the AIR as a function of SNR for different fiber lengths $L = \{1, 2, 5, 10\} \text{ km}$. These fiber lengths are chosen to cover a variety of scenarios, including the impact of selecting $W > 1$ and the transition from moderate to severe ISI. The results are organized into two columns. The first column corresponds to FD-RC pulse shaping ($\alpha_{\text{ps}} = 0.2$), while the second column corresponds to TD-RC pulse shaping ($\alpha_{\text{ps}} = 0.8$)⁶. The line style indicates the modulation format: Solid lines represent 4-PAM modulation ($M = 4$) while dashed lines represent 6-PAM modulation ($M = 6$). We compare the system performance with and without PM. The curves with marker \blacksquare represent results with PM and $W = 1$. Additionally, the curves marked with \star represent cases where

⁶A TD-RC pulse is not bandwidth-limited; however for $\alpha_{\text{ps}} = 0.8$, the 95% energy bandwidth is slightly larger than B , i.e., $1.2B$.

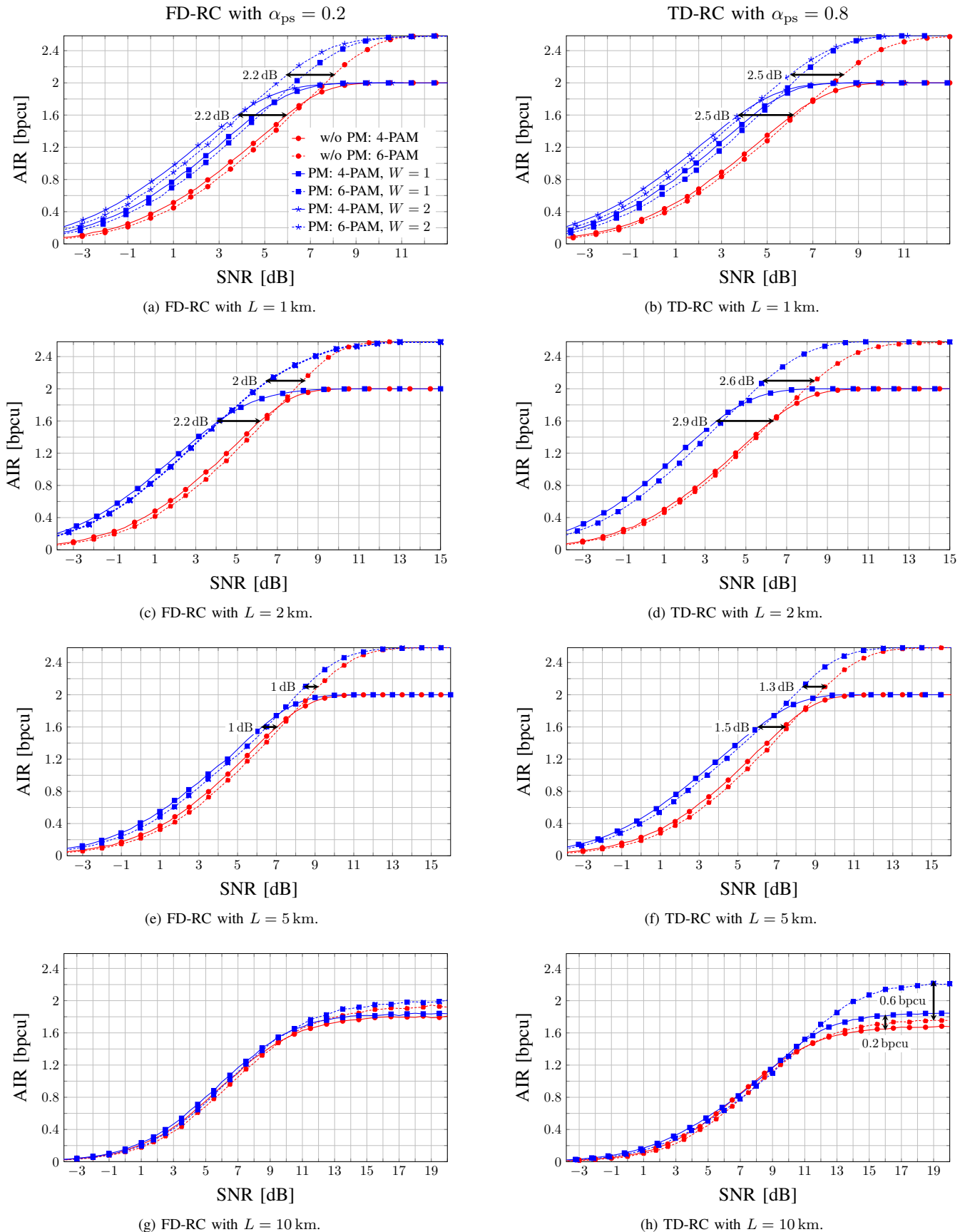


Fig. 5. AIR for FD-RC (left column), TD-RC (right column) and $L = \{1, 2, 5, 10\}$ km.

a second harmonic ($W = 2$) has notably improvement compared to $W = 1$. The marker \bullet stands for no PM. The legend in subplot (a) holds for all plots.

B. Impact of Phase Precoding

Consider first the curves without PM. For a fixed AIR, the required SNR grows as a function of the fiber length, which increases the total CD. At a certain fiber length, the system becomes interference-limited, where the maximal rate of $\log_2(M)$ bits cannot be achieved regardless of the SNR; see (g)-(h). Introducing phase precoding (\blacksquare , \star) improves the AIRs by mitigating CD, thereby reducing the required SNR to achieve a specific AIR. This can be seen in the plots (a)-(f) across both modulation formats. For instance, in plot (d), for $L = 2$ km, phase precoding results in an SNR gain of ≈ 3 dB for 4-PAM ($\text{---}\blacksquare\text{---}$) and ≈ 2.6 dB for 6-PAM ($\text{---}\star\text{---}$). Optimizing two coefficients (η_1, η_2) ($W = 2$: \star) gains an additional ≈ 0.6 dB over $W = 1$. However, with increasing fiber length this additional SNR gain decreases. For $L \geq 5$ km, CD becomes stronger and causes longer inter-symbol interference. For $L = 10$ km the system is interference-limited since the PM cannot compensate the CD that extends over several symbol periods; see plot (g) and (h). Here, FD-RC pulses show small AIR improvements in the high-SNR regime. For TD-RC and 6-PAM ($\text{---}\blacksquare\text{---}$), using a PM increases AIRs by 0.6 bpcu at high SNRs.

C. Limitations

The AIR gains of the PM are limited to moderate CD, or equivalently, moderate fiber lengths when operating at a fixed symbol rate. There are two reasons for this: First, the PM precodes phase only, but CD affects both phase and amplitude. Second, increasing CD causes longer inter-symbol interference, which cannot be compensated by a PM that precodes over a single symbol time slot T_s only.

V. CONCLUSION

We analyzed a low-cost PM for DD links. To optimize the phase modulator, we used a Fourier series representation of the periodic phase and adapted the closed-form expression from [6] for the mean-squared error (MSE) cost function. Numerical results show that the proposed scheme compensates CD for moderate fiber lengths, thus reducing the required transmit power. SNR gains of up to 3 dB are achieved when using 4-PAM modulation over $L = 2$ km.

Future work may explore phase precoding over multiple symbol slots. Additionally, adding a simple digital receive filter may further increase AIRs while keeping computational cost low.

ACKNOWLEDGMENTS

This work was carried out in the framework of the CELTIC NEXT Flagship project AI-NET PROTECT and was supported by the German Federal Ministry of Education and Research under the funding code FKZ16KIS1282.

APPENDIX

The gradient of (30) is

$$\frac{\partial \epsilon}{\partial \boldsymbol{\eta}} = -2 \xi^* \frac{\partial}{\partial \boldsymbol{\eta}} \mathbb{E}[S_\kappa Y_\kappa] + \xi^{*2} \frac{\partial}{\partial \boldsymbol{\eta}} \mathbb{E}[Y_\kappa^2], \quad (35)$$

with the terms

$$\begin{aligned} \frac{\partial}{\partial \boldsymbol{\eta}} \mathbb{E}[S_\kappa Y_\kappa] = & \quad (36) \\ & 2 \mu_S^2 \mathbf{g}^\top \text{Re}\{j[\mathbf{F}(\mathbf{u} \circ \boldsymbol{\Gamma})] \circ \mathbf{w}^*\} + \frac{\sigma_S^2}{2} \mathbf{g}^\top \text{Re}\{j(\mathbf{F} \circ \mathbf{A}) \boldsymbol{\Gamma}\} \\ & + \sigma_S^2 \mathbf{g}^\top \text{Re}\{j[\mathbf{F}(\mathbf{v} \circ \boldsymbol{\Gamma})] \circ \mathbf{w}^* - j[\mathbf{F}^*(\mathbf{u}^* \circ \boldsymbol{\Gamma})] \circ (\boldsymbol{\Psi} \mathbf{e}_{B_1})\}, \\ \text{and} \\ \frac{\partial}{\partial \boldsymbol{\eta}} \mathbb{E}[Y_\kappa^2] = & 4 \mu_S^2 \mathbf{g}^\top \text{Re}\{j[\mathbf{F}(\mathbf{u} \circ \boldsymbol{\Gamma})] \circ \mathbf{w}^*\} |\mathbf{w}|^{\circ 2, \top} \mathbf{g} \\ & + \sigma_S^2 \mathbf{g}^\top \text{Re}\{j \text{diag}(\mathbf{w}^*) \mathbf{F}[(\mathbf{N} \mathbf{d}) \circ \boldsymbol{\Gamma}] \\ & \quad - j \text{diag}(\boldsymbol{\Psi} \mathbf{d}) \mathbf{F}^*(\mathbf{u}^* \circ \boldsymbol{\Gamma})\} \\ & + \sigma_S^2 \mathbf{g}^\top \text{Re}\{j \text{diag}(\mathbf{w}^*) \mathbf{F}[(\mathbf{N} \mathbf{d}^*) \circ \boldsymbol{\Gamma}] \\ & \quad - j \text{diag}(\boldsymbol{\Psi} \mathbf{d}^*) \mathbf{F}^*(\mathbf{u}^* \circ \boldsymbol{\Gamma})\} \\ & + \sigma_S^2 \mathbf{g}^\top \text{Re}\{j(\mathbf{F} \circ \mathbf{A}) \boldsymbol{\Gamma} |\mathbf{w}|^{\circ 2, \top} + j([\mathbf{F}(\mathbf{u} \circ \boldsymbol{\Gamma})] \circ \mathbf{w}^*) \mathbf{z}^\top\} \mathbf{g} \\ & + \frac{\sigma_S^4}{8 \mu_S^2} \mathbf{g}^\top \text{Re}\{j[\mathbf{F} \circ (\mathbf{Q} \boldsymbol{\Psi} \mathbf{N}^\top)] \boldsymbol{\Gamma} + j[(\boldsymbol{\Psi} \mathbf{N}^\top) \circ (\mathbf{Q} \mathbf{F})] \boldsymbol{\Gamma}\} \\ & + \frac{\sigma_S^4}{8 \mu_S^2} \mathbf{g}^\top \text{Re}\{j[\mathbf{F} \circ (\mathbf{P} \boldsymbol{\Psi}^* \mathbf{N}^\top)] \boldsymbol{\Gamma} + j[(\boldsymbol{\Psi} \mathbf{N}^\text{H}) \circ (\mathbf{P} \mathbf{F}^*)] \boldsymbol{\Gamma}\} \\ & + \frac{\sigma_S^4}{4 \mu_S^2} \mathbf{g}^\top \text{Re}\{j(\mathbf{F} \circ \mathbf{A}) \boldsymbol{\Gamma}\} \mathbf{z}^\top \mathbf{g} \\ & + \frac{\mu_{4,S} - 3 \sigma_S^4}{4 \mu_S^2} \mathbf{g}^\top \text{Re}\{j(\mathbf{F} \circ \mathbf{B}) \boldsymbol{\Gamma}\}, \end{aligned} \quad (37)$$

and definitions

$$\begin{aligned} \mathbf{A} &= \boldsymbol{\Psi}^* \mathbf{N}^\top, \quad \mathbf{B} = [(\mathbf{g}^\top |\boldsymbol{\Psi}|^{\circ 2}) \circ \boldsymbol{\Psi}^*] \mathbf{N}^\top, \quad \mathbf{d} = \boldsymbol{\Psi}^\top \text{diag}(\mathbf{w}^*) \mathbf{g}, \\ \mathbf{N} &= (\mathbf{H} \circ \exp(j\boldsymbol{\varphi}')), \quad \mathbf{P} = (\boldsymbol{\Psi}^* \boldsymbol{\Psi}^\top) \circ \mathbf{g}^\top, \\ \mathbf{Q} &= (\boldsymbol{\Psi}^* \boldsymbol{\Psi}^\text{H}) \circ \mathbf{g}^\top, \quad \mathbf{u} = \mathbf{N} \mathbf{1}_K, \quad \mathbf{v} = \mathbf{N} \mathbf{e}_{B_1}, \end{aligned}$$

$\boldsymbol{\Gamma} \in \mathbb{R}^{M_f \times W}$ corresponding to (27) with

$$\boldsymbol{\Gamma} = \underbrace{[(\gamma_0, \gamma_1 \dots \gamma_{N_{\text{os}}-1})]}_{\text{Repeat } B_2 \text{ times}}, \gamma_0, \underbrace{(\gamma_1, \dots, \gamma_{N_{\text{os}}-1}, \gamma_0)}_{\text{Repeat } B_2 \text{ times}}]^\top. \quad (38)$$

REFERENCES

- [1] K. Zhang, Q. Zhuge, H. Xin, W. Hu, and D. V. Plant, "Performance comparison of DML, EML and MZM in dispersion-unmanaged short reach transmissions with digital signal processing," *Optics express*, vol. 26, no. 26, pp. 34 288–34 304, 2018.
- [2] M. Chagnon, "Optical communications for short reach," *J. Lightw. Technol.*, vol. 37, no. 8, pp. 1779–1797, 2019.
- [3] E. Ip, A. P. T. Lau, D. J. Barros, and J. M. Kahn, "Coherent detection in optical fiber systems," *Optics express*, vol. 16, no. 2, pp. 753–791, 2008.
- [4] L. Grüner-Nielsen, M. Wandel, P. Kristensen, C. Jorgensen, L. V. Jorgensen, B. Edvold, B. Pálsdóttir, and D. Jakobsen, "Dispersion-compensating fibers," *J. Lightw. Technol.*, vol. 23, no. 11, p. 3566, 2005.
- [5] M. Morsy-Osman, F. Fresi, E. Forestieri, M. Secondini, L. Poti, F. Cavaliere, S. Lessard, and D. V. Plant, "50 Gb/s short-reach interconnects with DSP-free direct-detection enabled by caps codes," *Opt. Express*, vol. 26, no. 14, pp. 17 916–17 926, 2018.

- [6] D. Plabst, F. J. G. Gómez, T. Wiegart, and N. Hanik, “Wiener filter for short-reach fiber-optic links,” *IEEE Commun. Lett.*, vol. 24, no. 11, pp. 2546–2550, 2020.
- [7] D. Plabst, T. Prinz, F. Diedolo, T. Wiegart, G. Böcherer, N. Hanik, and G. Kramer, “Neural network-based successive interference cancellation for non-linear bandlimited channels,” *IEEE Trans. Commun.*, to appear.
- [8] T. Wettlin, S. Calabrò, T. Rahman, J. Wei, N. Stojanovic, and S. Pachnicke, “DSP for high-speed short-reach IM/DD systems using PAM,” *J. Lightw. Technol.*, vol. 38, no. 24, pp. 6771–6778, 2020.
- [9] R. Killey, P. Watts, M. Glick, and P. Bayvel, “Electronic precompensation techniques to combat dispersion and nonlinearities in optical transmission,” in *2005 Europ. Conf. Opt. Commun.*, vol. 2. IET, 2005, pp. 251–254.
- [10] R. I. Killey, P. M. Watts, M. Glick, and P. Bayvel, “Electronic dispersion compensation by signal predistortion,” in *2006 Opt. Fiber Commun. Conf.* IEEE, 2006, pp. 3–pp.
- [11] D. Fonseca, A. Cartaxo, and P. Monteiro, “Transmission improvements using electrical dispersion compensation at the transmitter side and RZ pulse format in optical single sideband systems,” in *2005 Int. Conf. Transparent Opt. Netw.*, vol. 2. IEEE, 2005, pp. 381–384.
- [12] G. Goeger, “Modulation format with enhanced spm-robustness for electronically pre-distorted transmission,” in *2006 Europ. Conf. Opt. Commun.* IEEE, 2006, pp. 1–2.
- [13] R. I. Killey, P. M. Watts, V. Mikhailov, M. Glick, and P. Bayvel, “Electronic dispersion compensation by signal predistortion using digital processing and a dual-drive mach-zehnder modulator,” *IEEE Photon. Technol. Lett.*, vol. 17, no. 3, pp. 714–716, 2005.
- [14] M. J. Erro, M. Las, D. Benito, M. J. Garde, and M. A. Muriel, “A novel electrically tunable dispersion compensation system,” *IEEE J. Sel. Topics Quantum Electron.*, vol. 5, no. 5, pp. 1332–1338, 1999.
- [15] O. Mitomi, K. Wakita, and I. Kotaka, “Chirping characteristic of electroabsorption-type optical-intensity modulator,” *IEEE Photon. Technol. Lett.*, vol. 6, no. 2, pp. 205–207, 1994.
- [16] M. Y. Jamro and J. M. Senior, “Chirp control of an electroabsorption modulator to be used for regeneration and wavelength conversion at 40 Gbit/s in all-optical networking,” *Photonic Netw. Commun.*, vol. 10, pp. 267–278, 2005.
- [17] —, “Optimising negative chirp of an electroabsorption modulator for use in high-speed optical networks,” *Europ. Trans. Telecommun.*, vol. 18, no. 4, pp. 369–380, 2007.
- [18] P. Krehlik, “Directly modulated lasers in negative dispersion fiber links,” *Opto-Electron. Rev.*, vol. 15, no. 2, pp. 71–77, 2007.
- [19] C. del Río Campos and P. R. Horche, “Directly modulated laser intrinsic parameters optimization for WDM systems,” in *2008 Int. Conf. Advanc. Electron. and Micro-electron.* IEEE, 2008, pp. 78–83.
- [20] K. Sato, S. Kuwahara, and Y. Miyamoto, “Chirp characteristics of 40-Gb/s directly modulated distributed-feedback laser diodes,” *J. Lightw. Technol.*, vol. 23, no. 11, p. 3790, 2005.
- [21] N. Henmi, T. Saito, and T. Ishida, “Prechirp technique as a linear dispersion compensation for ultrahigh-speed long-span intensity modulation directed detection optical communication systems,” *J. Lightw. Technol.*, vol. 12, no. 10, pp. 1706–1719, 1994.
- [22] T. Preuschoff, P. Baus, M. Schlosser, and G. Birkl, “Wideband current modulation of diode lasers for frequency stabilization,” *Rev. Sci. Instrum.*, vol. 93, no. 6, 2022.
- [23] J. M. Wyrwas and M. C. Wu, “Dynamic range of frequency modulated direct-detection analog fiber optic links,” *J. Lightw. Technol.*, vol. 27, no. 24, pp. 5552–5562, 2009.
- [24] M. Imai and K. Kawakita, “Measurement of direct frequency modulation characteristics of laser diodes by michelson interferometry,” *Appl. Opt.*, vol. 29, no. 3, pp. 348–353, 1990.
- [25] S. Kobayashi, Y. Yamamoto, M. Ito, and T. Kimura, “Direct frequency modulation in AlGaAs semiconductor lasers,” *IEEE Trans. Microw. Theory Techn.*, vol. 30, no. 4, pp. 428–441, 1982.
- [26] M. Sanaee and A. Zarifkar, “Enhanced modulation and noise characteristics in 1.55 μm QD lasers using additional optical pumping,” *Int. J. Opt. Photonics*, vol. 11, no. 1, pp. 3–18, 2017.
- [27] D. Walker, H. Sun, C. Laperle, A. Comeau, and M. O’Sullivan, “960-km transmission over G. 652 fiber at 10 Gb/s with a laser/electroabsorption modulator and no optical dispersion compensation,” *IEEE Photon. Technol. Lett.*, vol. 17, no. 12, pp. 2751–2753, 2005.
- [28] M. Xu, M. He, Y. Zhu, S. Yu, and X. Cai, “Flat optical frequency comb generator based on integrated lithium niobate modulators,” *J. Lightw. Technol.*, vol. 40, no. 2, pp. 339–345, 2022.
- [29] R. Gallager, *Principles of Digital Communication*. Cambridge University Press, 2008.
- [30] D. Plabst, T. Prinz, T. Wiegart, T. Rahman, N. Stojanović, S. Calabrò, N. Hanik, and G. Kramer, “Achievable rates for short-reach fiber-optic channels with direct detection,” *J. Lightw. Technol.*, vol. 40, no. 12, pp. 3602–3613, 2022.
- [31] F. J. García-Gómez, “Numerically computing achievable rates of memoryless channels,” 2020.